Measuring the Single-Particle Density Matrix for Fermions and Hard-Core Bosons in an Optical Lattice

Luis A. Peña Ardila,[1,2,*] Markus Heyl,[1,†] and André Eckardt[1,‡]

[1]*Max Planck Institute for the Physics of Complex Systems, Nöthnitzer Straße 38, 01187 Dresden, Germany*
[2]*Institut for Fysik og Astronomi, Aarhus Universitet, 8000 Aarhus C, Denmark*

Ultracold atoms in optical lattices provide clean, tunable, and well-isolated realizations of paradigmatic quantum lattice models. With the recent advent of quantum-gas microscopes, they now also offer the possibility to measure the occupations of individual lattice sites. What, however, has not yet been achieved is to measure those elements of the single-particle density matrix, which are off- diagonal in the occupation basis. Here, we propose a scheme to access these basic quantities both for fermions as well as hard-core bosons and investigate its accuracy and feasibility. The scheme relies on the engineering of a large effective tunnel coupling between distant lattice sites and a protocol that is based on measuring site occupations after two subsequent quenches.

Introduction.—Atomic quantum gases in optical lattices [1–3] combine a variety of properties that make them a unique experimental platform for studying mesoscopic quantum phenomena. Primarily, these systems provide clean realizations of paradigmatic quantum lattice Hamiltonians, well isolated from the environment. Additionally, system parameters are highly adjustable including dimensionality, lattice geometry, interaction strengths, number of spin states, etc. Moroever, optical lattice systems offer also unique measurement capabilities beyond what is possible in solid-state systems. For example, using quantum-gas microscopes it is possible to measure the full spatial density profile with single-lattice-site resolution [4–12]. Upon repeating such experiments, one can determine means, fluctuations, correlations, and even full distribution functions of site occupations. This was used, e.g., to measure multiparticle string order [13,14]. Furthermore, combining these probes with measurement protocols, where additional dynamics is imposed, it has been achieved to detect entangled states of matter both by measuring a lower bound of the concurrence in spin systems [15,16] and by extracting Renyi entropies in one-dimensional (1D) bosonic lattice systems [17–19].

Yet, these quantum-gas microscopes provide direct access only to physical quantities (near) diagonal in the occupation basis. While protocols for measuring currents and coherences on neighboring lattice sites were proposed [20,21] and employed experimentally by either pairwise merging [22–24] or isolating [25] neighboring sites, the off-diagonal matrix elements of the single-particle density matrix (SPDM)

$$\chi_{\ell's',\ell s} = \langle \hat{c}^{\dagger}_{\ell's'} \hat{c}_{\ell s} \rangle, \qquad (1)$$

on distant non-neighboring lattice sites ℓ and ℓ' have not yet been accessed experimentally. Here, $\hat{c}_{\ell s}$ denotes the annihilation operator for a particle with spin s on lattice site ℓ. The SPDM contains elementary information about the physical properties of quantum many-body systems and therefore is of interest on general grounds. More specifically, one could use the SPDM to extract essential properties of many-body localized phases [26–28], to detect topological Mott insulating states [29], or to probe topological edge states [30]. Moreover, it can be used to reconstruct the full reduced density matrix of two lattice sites. This would allow us to access entanglement via the concurrence and the logarithmic negativity [31], to study signatures of the butterfly effect [32] or to detect many-body localized spin-glass order [33].

Here, we propose a feasible scheme for measuring the elements of the SPDM $\chi_{\ell's',\ell s}$ for fermions or hard-core bosons. Our approach requires the use of two techniques as they are available in the aforementioned quantum-gas microscopes: single-site resolved density measurements and the ability to design high-resolution light-shift potentials using digital mirror devices. Using these techniques we show (i) how two distant lattice sites $\ell' = a$ and $\ell = b$ can be isolated from the rest of the system and efficiently coupled to each other via virtual intermediate states forming a "channel" [Fig. 1(a)], and (ii) how to use this channel to measure $\chi_{\ell's',\ell s}$ by monitoring only local densities on a and b. The main result concerning point (i) is depicted in Fig. 1(e). It shows that the effective parameter for tunneling between a and b, B_x, whose inverse sets the measurement timescale, can be increased by orders of magnitude when structuring (optimizing) the potential landscape on the M sites between a and b [Fig. 1(c)]. This
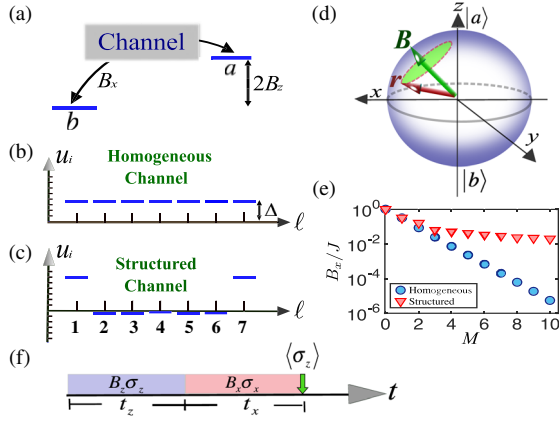

FIG. 1. (a) Two distant lattice sites a and b are effectively coupled to each other via energetically distant intermediate states of a channel formed by the sites between them. (b),(c) Homogeneous and structured (optimized) channel design: on-site potential u_ℓ on the sites $\ell = 1, \ldots, M$ between a and b, for $M = 7$ and $\epsilon = 0.05$. The horizontal axis defines zero energy $(u_a + u_b)/2 \equiv 0$, tick marks are separated by J. (d) Rotation of the pseudospin polarization r. (e) Effective tunnel coupling B_x vs M for $\epsilon = 0.05$. (f) Measurement protocol.

channel optimization is absolutely crucial, since for unstructured (homogeneous) channels [Fig. 1(b)] an exponential decay of B_x with M renders the measurement essentially impossible already for small distances. In turn, for the structured channel B_x scales like $1/M$ making measurements at longer distances much more feasible. In particular, this can allow for measuring all relevant single-particle matrix elements of (many-body) localized systems, involving distances roughly up to the localization length. For problem (ii) we design a measurement protocol that is based on monitoring the evolution of the densities on both sites after two subsequent quenches in the Hamiltonian. It goes beyond other quench-based measurement schemes [20,21,34–37] that were implemented already successfully in experiment [22–25,38–40]. In the following, we will first describe the measurement protocol (ii), then discuss the effective coupling of distant lattice sites (i), before closing with concluding remarks.

Measurement protocol.—We will first treat the case of spinless fermions, before addressing the spinful problem and the case of hard-core bosons. The SPDM on two sites a and b is then determined by

$$\chi_{ab} = \langle \hat{c}_a^\dagger \hat{c}_b \rangle = \mathrm{tr}\{\hat{\rho}\hat{c}_a^\dagger \hat{c}_b\}. \quad (2)$$

Here, $\hat{\rho}$ denotes the system's full density operator, which can either describe an equilibrium state or can result from a nonequilibrium process. As we show in more detail below, for our measurement protocol we engineer situations where the two sites a and b are isolated from the remainder of the system but still coupled to each other, such

that their dynamics is governed by two possible effective Hamiltonians:

$$\hat{H}_{ab}^z = B_z(\hat{n}_a - \hat{n}_b), \qquad \hat{H}_{ab}^x = B_x(\hat{c}_a^\dagger \hat{c}_b + \hat{c}_b^\dagger \hat{c}_a), \quad (3)$$

with $\hat{n}_\ell = \hat{c}_\ell^\dagger \hat{c}_\ell$, energy offset $2B_z$, and tunnel coupling B_x.

Let us first consider the subspace of a single fermion shared among both sites. It is convenient to introduce an effective pseudospin-1/2 representation with $\uparrow$ and $\downarrow$ referring to the cases where the fermion is located on site a and b, respectively. Then we can recast the reduced density matrix into the form $\hat{\rho}_{ab} = [1 + r \cdot \hat{\sigma}]/2$, with $\hat{\sigma} = (\hat{\sigma}_x, \hat{\sigma}_y, \hat{\sigma}_z)^t$ denoting the vector of Pauli matrices. It is characterized by the three-dimensional Bloch vector r of length $|r| \leq 1$ directly corresponding to the polarization, $\langle \hat{\sigma} \rangle = \mathrm{tr}(\hat{\rho}_{ab}\hat{\sigma}) = r$. The purity reads $\mathrm{tr}(\hat{\rho}_{ab}^2) = (1 + r^2)/2$, so that $|r| < 1$ for mixed states. The SPDM $\chi_{ab}^{(1)}$ in the one-fermion subspace is given by

$$\chi_{ab}^{(1)} = \mathrm{tr}(\hat{\rho}_{ab}|\downarrow\rangle\langle\uparrow|) = \langle\uparrow|\hat{\rho}_{ab}|\downarrow\rangle = (r_x - ir_y)/2. \quad (4)$$

Within the pseudospin representation, we can identify B_z and B_x as effective magnetic fields, i.e., $\hat{H}_{ab}^z = B_z\hat{\sigma}_z$, $\hat{H}_{ab}^x = B_x\hat{\sigma}_x$. Let us now consider a protocol, where we first evolve the system with $\hat{H}_{ab}^z$ for a time t_z and afterwards for a time t_x with $\hat{H}_{ab}^x$. This amounts to two successive spin rotations [Fig. 1(d)]: one by the angle $\alpha = B_z t_z/(2\hbar)$ around the z axis followed by one by the angle $\beta = B_x t_x/(2\hbar)$ around the x axis. It transforms the polarization r before the rotation, which we wish to reconstruct, to the rotated polarization $r' = r'(\alpha, \beta)$. Measuring the occupations n_a and n_b in repeated experiments, one can obtain the z polarization $r_z'(\alpha, \beta) = \langle \hat{n}_\uparrow - \hat{n}_\downarrow \rangle^{(1)}$ by averaging over the events with $n = n_a + n_b = 1$:

$$r_z'(\alpha, \beta) = \sin(\beta)[\sin(\alpha)r_x + \cos(\alpha)r_y] + \cos(\beta)r_z. \quad (5)$$

The measurement protocol is depicted in Fig. 1(f). From measuring $r_z'(\alpha, \beta)$ for different angles α and β, we can reconstruct r [and, using Eq. (4), also $\chi_{ab}^{(1)}$]:

$$r_x = r_z'(\pi/2, \pi/2), \quad r_y = r_z'(0, \pi/2), \quad r_z = r_z'(0,0). \quad (6)$$

Note that the parameters B_z and B_x, whose values control the angles α and β, do not need to be known before the experiment, but can be measured from the periodicity of r_z with respect to t_z and t_x. Note also that, in case we can assume that $\hat{\rho}_{ab}$ describes a pure state, $|r| = 1$, we can reconstruct r_y, r_z, and $|r_x| = [1 - r_y^2 - r_z^2]^{1/2}$ without the need of implementing a finite B_z for the α rotation. This has been exploited for the tomography of band insulators in momentum space [35,39].

Let us now discuss the general case where *a priori* any particle number $n = n_a + n_b$ can occur. When measuring the occupation numbers n_a and n_b, one first has to distinguish between the three possible outcomes $n = 0$, 1, 2, and note their relative frequencies p_n in repeated experiments. The cases $n = 0$ and $n = 2$ correspond to the states $|n_a n_b\rangle = |00\rangle$ and $|11\rangle$, respectively, which are invariant under the action of both Hamiltonians (3) and give $\chi_{ab}^{(0)} = \chi_{ab}^{(2)} = 0$ of $\hat{c}_a^\dagger \hat{c}_b$. Overall, the full SPDM element can thus be written as

$$\chi_{ab} = \sum_{n=0}^{2} p_n \chi_{ab}^{(n)} = p_1 \chi_{ab}^{(1)}. \tag{7}$$

The results obtained so far are equally valid for hard-core bosons, since $\chi_{ab}^{(0)} = \chi_{ab}^{(2)} = 0$ remains true and $\chi_{ab}^{(1)}$ is obtained from single-particle dynamics. The scheme does not generalize to soft-core bosons.

Finally, it is left to consider spinful fermions. The SPDM for equal spin states $\langle \hat{c}_{as}^\dagger \hat{c}_{bs} \rangle$ can be obtained by repeating the above protocol individually for each spin state. This requires spin-sensitive measurements of $\hat{n}_{as}$, as they were performed in various experiments. To obtain $\langle \hat{c}_{as'}^\dagger \hat{c}_{bs} \rangle$ for $s' \neq s$ one could first perform a spin rotation $s' \to s$ on site ℓ' and then, again, proceed as before. Since such a spin rotation commutes with both quench Hamiltonians, it could be performed also after the double quench. However, this is in turn equivalent to simply measuring $\hat{n}_{s'a}$ instead of $\hat{n}_{sa}$, so that actually no spin rotation is needed. Note that unlike for spinless fermions, which are noninteracting, the implementation of the quadratic Hamiltonians (3) requires for spinful fermions also to switch off the interactions using a Feshbach resonance [41]. This technique is available in a fermionic quantum-gas microscope [14].

Realizing the quench Hamiltonians.—Let us now discuss how to implement the Hamiltonians $\hat{H}_{ab}^z$ and $\hat{H}_{ab}^x$ experimentally. For simplicity, we will consider spinless fermions in 1D. The below reasoning applies also to hard-core bosons, which can be mapped to free fermions using a Jordan-Wigner transformation. For the spinful case the same Hamiltonian has simply to be realized for all spin components. The generalization to higher spatial dimensions can be achieved by realizing a 1D channel connecting two sites or, alternatively, by generalizing the below reasoning to higher-dimensional channel architectures.

We assume that during both stages of the measurement protocol the subsystem containing the two sites a and b as well as the M sites between them (forming the channel) is decoupled from the rest of the lattice by switching on a large potential offset. We label the lattice sites of this chain from a ($\ell = 0$) to b ($\ell = M + 1$) in ascending order:

$$\hat{H} = -J \sum_{\ell=a}^{b-1} (\hat{c}_\ell^\dagger \hat{c}_{\ell+1} + \hat{c}_{\ell+1}^\dagger \hat{c}_\ell) + \sum_{\ell=a}^{b} u_\ell \hat{n}_\ell. \tag{8}$$

Here, J denotes the tunneling amplitude and the u_ℓ are tunable on-site energies. The latter can be tuned independently using high-resolution light-shift potentials realized by digital mirror devices in quantum-gas microscopes. For later convenience let us decompose this Hamiltonian according to $\hat{H} = \hat{H}_{ab} + \hat{H}_{\mathrm{ch}} + \hat{H}_{\mathrm{cp}}$. Here, $\hat{H}_{ab} = u_a \hat{n}_a + u_b \hat{n}_b$ captures the subspace containing the sites $\ell = a, b$. The channel between a and b is described by the Hamiltonian $\hat{H}_{\mathrm{ch}} = -J \sum_{\ell=a+1}^{b-2} (\hat{c}_{\ell+1}^\dagger \hat{c}_\ell + \mathrm{H.c.}) + \sum_{\ell=a+1}^{b-1} u_\ell \hat{n}_\ell = \sum_k \alpha_k \hat{c}_k^\dagger \hat{c}_k$, which is diagonalized by the modes $k = 1, \ldots, M$, having energies α_k and annihilation operators $\hat{c}_k = \sum_{\ell=a+1}^{b-1} \lambda_{k\ell} \hat{c}_\ell$ with real coefficients $\lambda_{k\ell}$. The channel is coupled to a and b by $\hat{H}_{\mathrm{cp}} = -J(\hat{c}_a^\dagger \hat{c}_1 + \hat{c}_b^\dagger \hat{c}_M + \mathrm{H.c.}) = \sum_k (J_{ak} \hat{c}_a^\dagger \hat{c}_k + J_{bk} \hat{c}_b^\dagger \hat{c}_k + \mathrm{H.c.})$, where we defined the real matrix elements $J_{ak} = -J\lambda_{k(a+1)}$ and $J_{bk} = -J\lambda_{k(b-1)}$.

We aim at an effective Hamiltonian involving only the lattice sites a and b which we achieve by coupling them through the intermediate channel via virtual off-resonant processes. In this spirit, we consider a setup where the on-site energies u_ℓ are tuned in such a way that the tunneling from sites a and b into the channel is accompanied with a large energy cost. In this case, $\hat{H}_{\mathrm{cp}}$ constitutes a weak perturbation, that can be eliminated using a Schrieffer-Wolff transformation: $e^{\kappa \hat{S}}[\hat{H}_{ab} + \hat{H}_{\mathrm{ch}} + \kappa \hat{H}_{\mathrm{cp}}] e^{-\kappa \hat{S}} = \hat{H}_{ab}^{\mathrm{eff}} + \hat{H}_{\mathrm{ch}}^{\mathrm{eff}} + \mathcal{O}(\kappa^3)$, with counting parameter $\kappa = 1$ and an anti-Hermitian generator $\hat{S} = \sum_{k,x}(A_{xk} \hat{c}_x^\dagger \hat{c}_k - \mathrm{H.c.})$, which includes the small parameters of our approximation, $A_{xk} \equiv J_{xk}/(\alpha_k - u_x) \ll 1$ for $x = a, b$. This gives the effective Hamiltonian

$$\hat{H}_{ab}^{\mathrm{eff}} = B_x(\hat{c}_a^\dagger \hat{c}_b + \hat{c}_b^\dagger \hat{c}_a) + B_z(\hat{n}_a - \hat{n}_b), \tag{9}$$

with $2B_x = -\sum_k (A_{ak} J_{bk} + A_{bk} J_{ak})$ and $2B_z = u_a - u_b + \sum_k (A_{ak} J_{ak} - A_{bk} J_{bk})$, where we have dropped an irrelevant term $\propto (\hat{n}_a + \hat{n}_b)$. This Hamiltonian can take the form of both the desired quench Hamiltonians. For $u_a = u_b = 0$ one has $B_z = 0$ and $B_x = -\sum_k J_{ak} J_{bk}/\alpha_k$ so that $\hat{H}_{ab}^{\mathrm{eff}} = \hat{H}_{ab}^x$. In turn, $\hat{H}_{ab}^{\mathrm{eff}} \simeq \hat{H}_{ab}^z$ with $B_z = (u_a - u_b)/2$ can be achieved in the limit $A_{xk} \to 0$, which is reached by increasing the channel energies α_k via potentials u_ℓ.

Within our scheme there are two sources of errors. First, we neglect corrections in the perturbative derivation of the effective Hamiltonian beyond second order. Second, the effective Hamiltonian is not realized in the basis of bare site occupations, but rather in the slightly rotated perturbed basis. The second error is of second order (as we argue now) and therefore dominates. Considering $u_a = u_b = 0$ as well as a reflection-symmetric channel Hamiltonian (so that $A_{ak}^2 = A_{bk}^2$) and assuming that terms containing off-diagonal expectation values $\langle \hat{c}_a^\dagger \hat{c}_k \rangle$ and $\langle \hat{c}_{k'}^\dagger \hat{c}_k \rangle$ with $k' \neq k$ sum up to zero (rotating wave approximation), we find
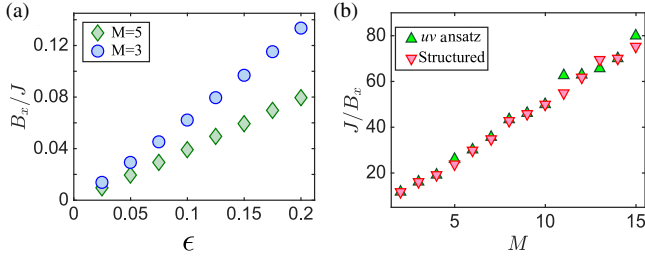
FIG. 2. (a) Effective coupling versus the estimated error. (b) Inverse effective coupling versus channel length.

$$\langle e^{\hat{S}}(\hat{n}_a - \hat{n}_b)e^{-\hat{S}}\rangle = (1 - \epsilon)\langle(\hat{n}_a - \hat{n}_b)\rangle,$$ with the state-independent relative error between dressed and bare z polarization

$$\epsilon = \sum_k A_{ak}^2. \qquad (10)$$

In the following, we optimize our channel in such a way that we maximize B_x while keeping the target error ϵ fixed. We also confirm numerically that the estimated error ϵ indeed quantifies deviations between the exact time evolution and that generated by the effective Hamiltonian.

Engineering the channel.—Let us first consider a homogeneous channel [Fig. 1(b)] with $u_\ell = \Delta \gg J$, giving rise to channel states with energies $\alpha_k = \Delta - 2J\cos[\pi k/(M+1)]$ and wave functions $\lambda_{k\ell} = [2/(M+1)]^{1/2}\sin[\pi k\ell/(M+1)]$ on the sites $\ell = 1, ..., M$ of the channel (for convenience, we assume $a = 0$). Choosing Δ for each M so that $\epsilon = 0.05$, we find an exponential suppression of B_x with M [Fig. 1(e), circles], related to a destructive interference between channel modes. Namely B_x is a sum over terms with oscillating sign, since $\lambda_{kM} = (-)^{k+1}\lambda_{k1}$. This unfavorable scaling restricts the scheme to short distances.

To obtain better results, we investigate structured reflection-symmetric channel potentials u_i [Fig. 1(c)]. We maximize B_x again under the constraint $\epsilon = 0.05$ [42]. Figure 1(c) shows the optimized channel design for $M = 7$. We find a power law instead, $B_x \sim 1/M$ [Fig. 2(b), triangles]. This tremendous improvement is one of the main result of this Letter. It implies that significant effective coupling matrix elements can be engineered over rather large distances. Figure 2(a) shows that the optimized coupling B_x scales proportional to the error.

Let us study the validity of our perturbative results and compare the evolution of the z polarization $\langle(\hat{n}_a - \hat{n}_b)\rangle$ generated by the full Hamiltonian $\hat{H}_{ab} + \hat{H}_{ch} + \hat{H}_{cp}$ to the one obtained from the effective Hamiltonian $\hat{H}_{ab}^{eff} = \hat{H}_{ab}^x$. Two examples are shown in Fig. 3(a). Fitting $A\sin(\omega t - \eta)$ to the exact evolution, we can compare the extracted amplitude A and phase η (ω to the perturbative results A_{eff} and η_{eff}. In Figs. 3(c) and 3(d) we plot the errors $\epsilon_{amp} = |A - A_{eff}|/|A|$ and $\epsilon_{ph} = |\eta - \eta_{eff}|$ versus the initial polarization r, characterized by $|r| = 1$ and polar angles (θ, ϕ). Their behavior with respect to the estimated error ϵ is
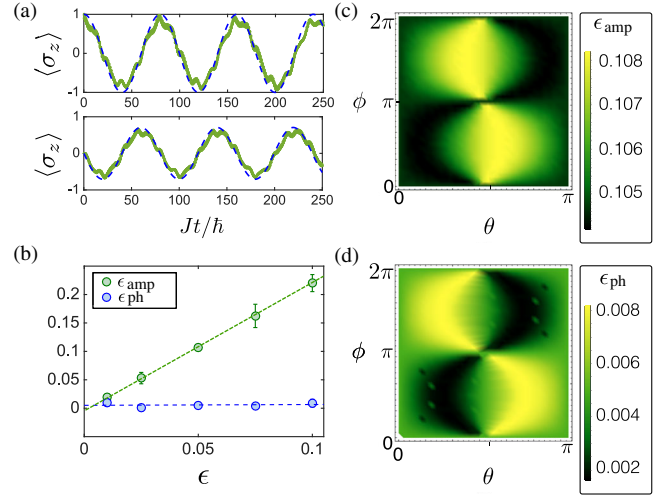

FIG. 3. (a) Evolution of z polarization for full and effective Hamiltonian (solid and dashed lines, respectively) for $\epsilon = 0.05$, and initial polarizations $(\theta, \phi) = (0, \pi/4)$ (upper) and $(\pi/2, \pi/4)$ (lower). (b) Amplitude and phase error (averaged over initial polarization with fluctuations indicated by error bars) versus estimated error. (c),(d) Amplitude and phase error versus initial polarization for $\epsilon = 0.05$. In all panels (a)–(d) $M = 5$ and $|r| = 1$.

depicted in Figs. 3(b). The amplitude error ϵ_{amp} is directly related to the estimated error ϵ. Like ϵ it (practically) does not depend on the state [see limits of color bar in Fig. 3(c)] and we find a linear scaling $\epsilon_{amp} \approx 2\epsilon$ [Fig. 3(b)], consistent with the fact that projecting between bare and the perturbed basis states leads to an error twice (when switching on $\hat{H}_{ab}^x$ and when recording bare site occupations afterwards). The phase error is much smaller [$\lesssim 10^{-2}$, see Fig. 3(d)] and does not show a strong dependence on ϵ. This justifies *a posteriori* our choice to quantify the error via ϵ.

Finally, we wish to shed light on the physics underlying the $1/M$ scaling of B_x. For this purpose, we consider a simple model for a structured channel and show that it gives rise to such behavior. Motivated by the results of the channel optimization [see Fig. 1(c) for the $M = 7$], we define $u_1 = u_M = u$ and $u_2 = \cdots = u_{M-1} = v$. The energy v shall be comparable to J, while u takes a large value forming a barrier at both channel edges. In this way tunneling from a (b) into the central channel ($i = 2, ..., M - 1$) via the edge site 1 (M) can be viewed as a second-order process with effective matrix element $-J_{eff} \approx J^2/u$. Diagonalizing the homogeneous central channel, we obtain modes $q = 1, ..., M - 2$ with energies $\beta_q = v - 2J\cos[\pi q/(M-1)]$. The maximum energy separation from neighboring levels $\Delta\beta \approx 2\pi J/M$ is found for modes $q \approx (M - 1)/2$; let q_0 be one of them. By tuning u and v, we can achieve that $|J_{eff}\lambda| \ll |\epsilon_{q_0}| \ll \Delta\beta$, where $\lambda \approx \sqrt{2/M}$ and $(-)^{q_0+1}\lambda$ are the overlaps of mode q_0 with site $i = 2$ and $i = M - 1$, respectively. Let us say, $\epsilon_{q_0} = \delta\Delta\beta$

and $J_{\mathrm{eff}}\lambda = \delta^2 \Delta\beta$, with small parameter $|\delta| \ll 1$. This corresponds to a situation, where both sites a and b couple to each other predominantly through a single central channel mode q_0, so that destructive interference between channel modes is avoided. Now, we can estimate B_x as resulting from a second-order process on a next level, connecting a and b via the intermediate virtual state q_0. We find $B_x \approx (-)^{q_0} \lambda^2 J_{\mathrm{eff}}^2 / \epsilon_{q_0} \propto J/M$. Computing B_x within this ansatz by optimizing u and v for each system size M, keeping $\epsilon = 0.05$ fixed, clearly confirms the linear scaling of J/B_x with M [Fig. 2(b), green triangles]. Surprisingly, the uv ansatz works almost as well as the full channel optimization (red triangles), which also give large barrier potentials $u_1 = u_M$. Thus, apart from providing insight into the mechanism underlying the channel architecture, the uv ansatz provides also a simple recipe for the experimental implementation of our measurement scheme.

Conclusions.—In summary, we have proposed an experimental scheme for measuring off-diagonal elements of the SPDM in lattice-site representation for fermions and hard-core bosons in optical lattices. It relies on the ability of quantum-gas microscopes to both measure occupations and create light-shift potentials with single-site resolution. For this purpose we showed on the one hand, how to engineer a significant effective tunnel coupling between distant lattice sites. On the other hand, we presented a protocol that uses the dynamics induced by suddenly switching on this coupling for reconstructing the sought-after matrix elements between two sites ℓ and ℓ' from measuring the occupations on these sites only.

---

*luis@phys.au.dk
†heyl@pks.mpg.de
‡eckardt@pks.mpg.de

[1] I. Bloch, J. Dalibard, and W. Zwerger, Rev. Mod. Phys. **80**, 885 (2008).
[2] M. Lewenstein, A. Sanpera, and V. Ahufinger, *Ultracold Atoms in Optical Lattices: Simulating Quantum Many-Body Systems* (Oxford University, New York, 2012).
[3] C. Gross and I. Bloch, Science **357**, 995 (2017).
[4] W. S. Bakr, J. I. Gillen, A. Peng, S. Foelling, and M. Greiner, Nature (London) **462**, 74 (2009).
[5] J. F. Sherson, C. Weitenberg, M. Endres, M. Cheneau, I. Bloch, and S. Kuhr, Nature (London) **467**, 68 (2010).
[6] L. W. Cheuk, M. A. Nichols, M. Okan, T. Gersdorf, V. V. Ramasesh, W. S. Bakr, T. Lompe, and M. W. Zwierlein, Phys. Rev. Lett. **114**, 193001 (2015).
[7] M. F. Parsons, F. Huber, A. Mazurenko, C. S. Chiu, W. Setiawan, K. Wooley-Brown, S. Blatt, and M. Greiner, Phys. Rev. Lett. **114**, 213002 (2015).
[8] E. Haller, J. Hudson, A. Kelly, D. A. Cotta, B. Peaudecerf, G. D. Bruce, and S. Kuhr, Nat. Phys. **11**, 738 (2015).
[9] G. J. A. Edge, R. Anderson, D. Jervis, D. C. McKay, R. Day, S. Trotzky, and J. H. Thywissen, Phys. Rev. A **92**, 063406 (2015).
[10] A. Omran, M. Boll, T. A. Hilker, K. Kleinlein, G. Salomon, I. Bloch, and C. Gross, Phys. Rev. Lett. **115**, 263001 (2015).
[11] C. Groß, Nat. Photonics **9**, 482 (2015).
[12] S. Kuhr, Natl. Sci. Rev. **3**, 170 (2016).
[13] M. Endres, M. Cheneau, T. Fukuhara, C. Weitenberg, P. Schauß, C. Gross, L. Mazza, M. Bañuls, L. Pollet, I. Bloch, and S. Kuhr, Science **334**, 200 (2011).
[14] T. A. Hilker, G. Salomon, F. Grusdt, A. Omran, M. Boll, E. Demler, I. Bloch, and C. Gross, Science **357**, 484 (2017).
[15] L. Mazza, D. Rossini, R. Fazio, and M. Endres, New J. Phys. **17**, 013015 (2015).
[16] T. Fukuhara, S. Hild, J. Zeiher, P. Schauß, I. Bloch, M. Endres, and C. Gross, Phys. Rev. Lett. **115**, 035302 (2015).
[17] C. M. Alves and D. Jaksch, Phys. Rev. Lett. **93**, 110501 (2004).
[18] A. J. Daley, H. Pichler, J. Schachenmayer, and P. Zoller, Phys. Rev. Lett. **109**, 020505 (2012).
[19] R. Islam, R. Ma, P. M. Preiss, M. E. Tai, A. Lukin, M. Rispoli, and M. Greiner, Nature (London) **528**, 77 (2015).
[20] M. Killi, S. Trotzky, and A. Paramekanti, Phys. Rev. A **86**, 063632 (2012).
[21] S. Keßler and F. Marquardt, Phys. Rev. A **89**, 061601 (2014).
[22] S. Trotzky, P. Cheinet, S. Fölling, M. Feld, U. Schnorrberger, A. M. Rey, A. Polkovnikov, E. A. Demler, M. D. Lukin, and I. Bloch, Science **319**, 295 (2008).
[23] S. Nascimbène, Y.-A. Chen, M. Atala, M. Aidelsburger, S. Trotzky, B. Paredes, and I. Bloch, Phys. Rev. Lett. **108**, 205301 (2012).
[24] D. Greif, T. Uehlinger, G. Jotzu, L. Tarruell, and T. Esslinger, Science **340**, 1307 (2013).
[25] S. Trotzky, Y. Chen, I. P. McCulloch, U. Schollwöck, J. Eisert, and I. Bloch, Nat. Phys. **8**, 325 (2012).
[26] S. Bera, H. Schomerus, F. Heidrich-Meisner, and J. H. Bardarson, Phys. Rev. Lett. **115**, 046603 (2015).
[27] S. Bera, T. Martynec, H. Schomerus, F. Heidrich-Meisner, and J. H. Bardarson, Ann. Phys. (Berlin) **529**, 1600356 (2017).
[28] T. L. M. Lezama, S. Bera, H. Schomerus, F. Heidrich-Meisner, and J. H. Bardarson, Phys. Rev. B **96**, 060202 (2017).
[29] S. Raghu, X.-L. Qi, C. Honerkamp, and S.-C. Zhang, Phys. Rev. Lett. **100**, 156401 (2008).
[30] Y.-C. He, F. Grusdt, A. Kaufman, M. Greiner, and A. Vishwanath, Phys. Rev. B **96**, 201103 (2017).
[31] M. B. Plenio and S. S. Virmani, in *Quantum Information and Coherence*, edited by E. Andersson and P. Öhberg (Springer, New York, 2014), pp. 173–209.
[32] X. Chen, T. Zhou, and C. Xu, J. Stat. Mech. 2018, 073101.
[33] Y. Javanmard, S. Bera, and M. Heyl, arXiv:1806.02571.
[34] M. Ohliger, V. Nesme, and J. Eisert, New J. Phys. **15**, 015024 (2013).
[35] P. Hauke, M. Lewenstein, and A. Eckardt, Phys. Rev. Lett. **113**, 045303 (2014).

[36] C. Wang, P. Zhang, X. Chen, J. Yu, and H. Zhai, Phys. Rev. Lett. **118,** 185701 (2017).

[37] M. Gluza, T. Schweigler, B. Rauer, C. Krumnow, J. Schmiedmayer, and J. Eisert, arXiv:1807.04567.

[38] M. Atala, M. Aidelsburger, M. Lohse, J. T. Barreiro, B. Paredes, and I. Bloch, Nat. Phys. **10,** 588 (2014).

[39] N. Fläschner, B. S. Rem, M. Tarnowski, D. Vogel, D.-S. Lühmann, K. Sengstock, and C. Weitenberg, Science **352,** 1091 (2016).

[40] M. Tarnowski, F. N. Ünal, N. Fläschner, B. S. Rem, A. Eckardt, K. Sengstock, and C. Weitenberg, arXiv:1709.01046.

[41] C. Chin, R. Grimm, P. Julienne, and E. Tiesinga, Rev. Mod. Phys. **82,** 1225 (2010).

[42] For each set of channel parameters u_i, we diagonalize the channel Hamiltonian and compute both B_x and ϵ using the expressions obtain from perturbation theory.